A 2D Model to describe the mechano-sensory behaviour of self-supporting shoots of climbing plants against gravity

Giacomo Vecchiato[1,a], Tom Hattermann[2,b], Michele Palladino[1,3,c], Fabio Tedone[1,d], Patrick Heuret[2,e], Nicholas P. Rowe[2,f], and Pierangelo Marcati[1,g]

[1]Gran Sasso Science Institute, L'Aquila, Italy
[2]AMAP, Univ Montpellier, CIRAD, CNRS, INRAe, IRD, Montpellier, France
[3]DISIM, Department of Information Engineering, Computer Science and Mathematics, University of L'Aquila, Via Vetoio - 67100 L'Aquila, Italy
[a]giacomo.vecchiato@gssi.it
[b]tom.hattermann@gmail.com
[c]michele.palladino@gssi.it
[d]fabio.tedone@gssi.it
[e]patrick.heuret@inrae.fr
[f]nicholas.rowe@cirad.fr
[g]pierangelo.marcati@gssi.it

Abstract

Climbing plants exhibit specialized shoots, called "searchers", to cross spaces and alternate between spatially discontinuous supports in their natural habitats. To achieve this task, searcher shoots combine both primary and secondary growth processes of their stems in order to support, orientate and explore their extensional growth into the environment. Currently, there is an increasing interest in developing models to describe plant growth and posture. However, the interactions between the sensing activity (e.g. photo-, gravi-, proprioceptive sensing) and the elastic responses are not yet fully understood. Here, we aim to model the extension and rigidification of searcher shoots. Our model defines variations in the radius (and consequently in mass distribution) along the shoot based on experimental data collected in natural habitats of two climbing species: *Trachelospermum jasminoïdes* (Lindl.) Lem. and *Condylocarpon guianense* Desf.. Using this framework, we predicted the sensory aspect of plant, that is, the plant's response to external stimuli, and the plant's proprioception, that is, the plant's "self-awareness". The results suggest that the inclusion of the secondary growth in a model is fundamental to predict the postural development and self-supporting growth phase of shoots in climbing plants.

1

Author Summary

Plant growth is influenced by many external and internal factors, such as light, gravity, structural flexibility of the stem or hormone fluxes. In recent years, plant movements and modelization have received an increasing attention, leading to a better understanding of plant development. In this work, we introduce a 2D model for self-supporting structures developed by climbing plants. This model is in the direction of filling the gap that currently exists between models for plant sensing activity and models focused on the mechanical aspect of plant growth. Indeed, we consider the response of the plant to external cues together with the capability of the plant to perceive itself (proprioception) and the radial expansion process (secondary growth). We then see how to retrieve the model parameters from a minimal set of experimental data and finally test the model by comparing its numerical simulations with real plant shapes. Our result shows that a better consideration of mass distribution along the shoot is important to understand the shape of self-supporting structures.

1   Introduction

The seminal work of Charles Darwin (1865) on the support-searching movements of climbing plants opened up new paths of thinking on plant life histories. Known to be the longest plants on land, climbing plants exhibit a wide diversity of mechanical architectures and ecological strategies [1] across many different phylogenetic groups [2]. Unlike trees that remain self-supporting throughout their entire life cycle, climbing plants are well-known for relying on physical support to grow vertically and towards light. To exploit supports, climbing plants rely on a developmental phase, known as "searcher shoot", which is specialized in crossing gaps, and searching and attaching to supports [3, 4]. To achieve these tasks, searcher shoots combine primary and secondary growth processes and actively modulate their development according to internal and external stimuli [5]. For example, it is well known how the contact with a support induces specific growth responses (i.e. thigmomorphogenesis), but it remains poorly understood how searcher shoot respond and interact with gravity during different kinds of exploratory tasks, such as growing in a specific direction or exploring volumes by circumnutational movements.

1.1   Plant shape and movement as a stimuli-response phenomenon

The responses that led to a turning movement and alignment of growth of a plant organ with respect to external vectorial cues have been known for many years as *tropisms* [6, 7]. A plant organ may tend to orient or grow towards a

stimulus (positive tropism), or away from it (negative tropism) [8]. For example, many aerial shoots of plants grow upwards against gravity whereas most roots tend to grow downwards [7] to locate the ground. Both organs perceive gravity via modified plastids (statholits) within specialised cells (statocytes), but the growth responses are induced by different biochemical signalling and auxin flux carriers [9, 10]. Supported by mathematical analysis and models, the gravitational responses have been linked with the statholits sedimentation, as well as the diffusion of auxin, and they are considered in terms of differential growth within the plant body [11, 12, 13, 14]. Given the complexity of interaction between the growing activity of plants and external and internal cues, growth movements can be viewed as an integrative response to diverse specific stimuli-response processes.

1.2 Brief review of mathematical models

One of the earliest studies investigating the stimuli-response behaviour in plants was carried out by Julius Sachs in 1882 [15]. As a result of his observations, the formation of curvatures along the plant body against gravity had first only been linked to gravity perception during primary growth. The upward bending movement of the shoot being stronger in the horizontal position then the vertical one has been described according to the "sine law" because it can be reformulated with the relation $\partial_t \kappa \propto \sin \theta$. Here $\partial_t \kappa$ is the curvature change rate and θ is the inclination of the stem. This fundamental relation between curvature and inclination has remained in the biological cultural framework for over a century. Only in 2013 the mathematical studies of Bastien et al. [16] demonstrated that if the phenomenon of the response to gravity is described only on the base of the sine law, the plant can never reach a vertical steady state. This is due to infinite lateral oscillations that would arise during the upward growth of the shoot. To stabilise the self-supporting system, the sine law was modified with a positive proprioceptive term, becoming $\partial_t \kappa \approx \sin \theta - \kappa$. This additional term tends to regulate high curvature κ towards 0 in time.

In parallel with the sensing activity of the plants, a wide literature has been developed on the physical and mechanical properties of shoot growth [17, 18, 19, 20, 21, 22, 23]. Knowledge of developmental changes and physical parameters, such as diameter, length and stiffness have been considered as the main descriptors of the stem shape. Founded on the Euler-Bernoulli beam theory, these mathematical models assume that a plant shoot behaves as a growing elastic rod, and they are mainly based on two configurations: (i) the current configuration, which corresponds to the actual shape of the elastic rod when subject to gravity or any external forces, and (ii) the relaxed or intrinsic configuration, that is the shape of the rod in the weightless limit case. In particular, in case (ii), the shape of the rod is described by a purely geometric evolution equation, which neglects mechanical effects. Further details about these configurations are given in section 2.1.

Recent studies have also combined analysis on gravitropism and proprioception along with studies on the mechanics of growth, including a planar model

3

of a growing plant [24]. Here the elastic rod is subject to the effects of gravity and develops according to the sine law corrected via a proprioceptive term as proposed in [16]. Some excellent guidelines in the modelisation of the sensing activity and its interaction with the plant growth mechanics can be found in [25, 26, 27].

In these models the formation and the growth of tissue layers, resulting from the secondary growth, together with the development of the intrinsic curvature in function of the shoot inclination and the proprioception have never been considered [27]. For example, some models have included a linear density parameter ρ, which is constant along the stem and doesn't change over time (for instance, [11, 24]). This potentially limits two important features characterising actual shoot growth: first, it assumes that the shape, the size of the stem cross-section and any internal growth expansion of mechanical tissue (e.g., of the wood cylinder) remain constant over time. Second, it does not take into account the build-up of mass along the the shoot due to secondary growth of the wood cylinder and other tissues. Early development of additive growth, maturation and stiffening of mechanical tissue via early secondary growth are key development features in plant shoots in general and especially in young searcher shoots of climbing plants [28, 29, 30]. Stem stiffness and rigidity can be significantly modified by even small changes of expansion of the wood cylinder within the primary body of the plant stem even before noticeable changes in external stem diameter [3]. However, this is only one of the possible ways in which a searcher shoot can adjust its mechanical properties. From its base to the apex, a shoot can adjust its rigidity by decreasing the radius, modifying the structure and the chemistry of tissues [31] or modifying the gradient of tissue stiffness along the stem. The complexity of the interaction between all these mechanisms likely leads to a very complicated gradient of organisation, which are arguably difficult to capture or integrate using a single unifying model.

1.3   Purpose of the study

The aim of this study is to display the relevance of the mechanics in the behaviour of a climbing plant searcher shoot, considering in particular the radial expansion of the main stem. To this end, we first develop a mathematical model able to capture a variety of shapes and orientations observed in climbing plant searchers; second, we develop an approach to reconstruct extensional growth against gravity from a static description of the shoot final state. This approach aims to use a minimal number of parameters, which can be relatively easily obtained from field observations of different species with variable behaviours. In particular, we aim to show how the interplay between variable linear density, proprioception and external stimuli can generate shape and orientations of searcher shoots in two different climbing plants species in the family of Apocynaceae: *Trachelospermum jasminoïdes* (Lindl.) Lem. and *Condylocarpon guianense* Desf. These relatively close-related species have been chosen because they share some fundamental properties during their searching and twining growth behaviour. Both species (i) attach to support by twining; (ii) are capable of

4

reaching similar maximal reach capacities of around 110 cm in length (iii) and have similar values of structural Young's modulus at the base of searcher shoots of around 3000 $N\,m^{-2}$ [29, 30].

In order to model a generically directed stimulus we consider the equations used by Guillon et al. [21] corrected with the proprioceptive term introduced by Bastien et al. [16]. The resulting growth dynamics is addressed through numerical simulations. Some recent studies have used numerical tools based on arbitrary parameters to illustrate generic mechanical behaviours through simulations [11, 24, 12]. Rather than arbitrarily calibrating every parameter, we set their order of magnitude using measured data from two climbing plant species *T. jasminoïdes* and *C. guianense* growing in natural conditions. This enabled us to calibrate the morphological parameters as well as the measurements of internode length at different times, which were crucial for estimating the growth parameters.

1.4 Glossary

In this study, we use some technical terms that might not be familiar or that need clarification for a diverse scientific community. To avoid confusion, we present a short glossary here.

Searcher shoot: The developmental phase of a climbing plant responsible for spanning gaps, foraging for support and attaching. A searcher shoot always includes a main axial structure (most often a stem) which is mechanically self-supporting from the base. According to the species, it may bear different structures such as leaves, and branches, as well as structures modified into attachment systems such as tendrils and stem segments capable of twining. Searcher stems can often undergo growth-induced movements specialized in exploring its vicinity and support attachment.

Reach: The effective length observed between the apical tip of a searcher shoot and the basal point from which it is attached or fixed (see figure 1a). Maximal reach can be viewed as a functional descriptor of searcher-shoot gap-spanning capacity in a functional and ecological context.

Orientation: The slope of the line joining the base with the tip of a searcher stem in a vertical plan. Here, the orientation was measured only at the final configuration when the searcher shoot was estimated to have attained its maximal reach in a self-supporting state (see figure 1a).

Primary Growth: The increase in growth results from cell division in the apical meristem of axes and subsequent cell elongation and maturation. These lead to the growth in length of the searcher stem. In this paper we use the term *extension* as the morphogenetic additive process leading to the "lengthening" of a shoot during primary growth. Hence, the term describes a macroscopic phenomenon that implicitly includes smaller-scale growth processes such as: cell initiation, multiplication, differentiation and maturation.

Secondary Growth: The increase in growth that results from cell division by the vascular cambium; a ring-like meristematic tissue producing wood (secondary xylem and ray tissue) and secondary phloem. Subsequent expansion and
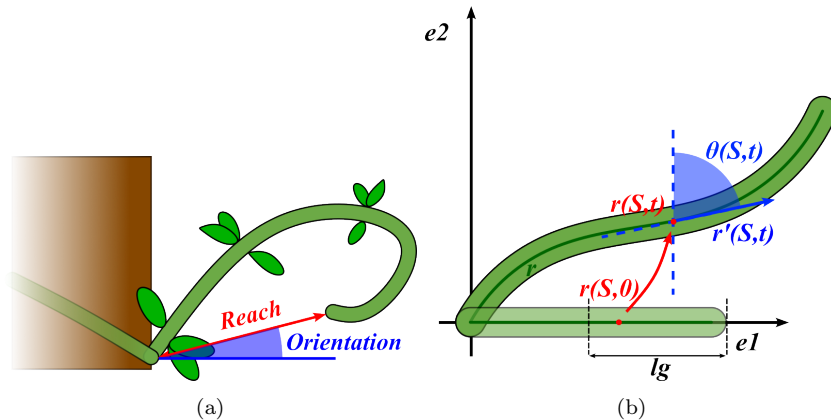
Figure 1: (1a): Reach and orientation in searcher stems. Measurement of reach and orientation in a typical searcher shoot of a climbing plant. The reach is measured as a straight line form the base of the searcher stem at its point of attachment with the parent bearing stem to the curved hook-like apex. It represents the effective distance a self-supporting searcher stem often capable of movement towards the apex. The orientation is the slope of that joining line with respect to the horizontal line.

(1b): Schematic illustration of the curve elaborated by the mathematical model. At each time t of searcher shoot growth, the mathematical model represents its position in the space with a curve r. In the figure, e_1 and e_2 are the two orthogonal vectors that span the plane in which the curve is confined. So, these vectors correspond respectively to the (x, y) coordinates of the curve. For a given time t, any point of the curve is identified with the vector $r(S, t)$, where S is a parameter which varies in $[0, \ell_0]$. The figure shows that the mathematical model leads the point of the curve at time zero with position $r(S, 0)$ to the point at time t with position $r(S, t)$. Each point $r(S, t)$ of the curve has a certain inclination to the vertical line, denoted by $\theta(S, t)$. ℓ_g is the parameter used by the model as length of the extension zone. The sensing equation and the growth involve only the points of that zone.

maturation of additionally formed cells leads to a radial thickening of the stem.
Rigidification: The phenomenon of stem thickening and stiffening that can be achieved by radial growth and cell maturation. Here, changes in geometry and material properties of the stem are implicitly considered.
Proprioception: The capability of the shoot to perceive changes in shape and orientation in terms of curvature and to respond to these changes in order to restore local straightness.

2   Materials and Methods

2.1   Formulation of the model

The searcher stem is modeled as an unshearable and elastically inextensible rod. We consider the curve r identifying the centreline of the rod to be confined in a plane spanned by two orthonormal vectors $\{e_1, e_2\}$. We assume that the curve

r is parametrized with respect to its arc length $s \in [0, \ell(t)]$, where $\ell(t)$ is the length of the curve at time $t \in [0, T]$. We call $\ell_0 = \ell(0)$ the initial length of the curve r. The change over time of the total length is due to the extension process that takes place in a region of finite length ℓ_g located at the apex of the plant (see Figure 1b). The points of the plane $\{e_1, e_2\}$ that at time t belongs to r are uniquely identified by s and we indicate them with $r(s, t)$. In the terminology used in the introduction, $r(s, t)$ can be regarded as the position of the current configuration of the curve. Since we assume that the curve evolution is confined in the plane spanned by $\{e_1, e_2\}$, it is convenient to describe the position of the curve using the angle $\theta(s, t)$ between the tangent vector at the point $r(s, t)$ and the vertical line e_2 (see Figure 1b). In particular, the curvature of the curve at the point $r(s, t)$ is provided by $\partial_s \theta(s, t)$, where ∂_s denotes the partial derivative with respect to s. To describe the elongation process, we consider another parametrization of the curve which is independent of time t. By calling $S \in [0, \ell_0]$ the arc length parameter of the curve at the initial time, the parameter s can be considered as a function of S and t. Indeed, as long as $s(S, t)$ is inside the extension zone, the infinitesimal ratio $\frac{\partial s}{\partial S}(S, t)$ increases uniformly at rate G_0 according to the following equation:

$$G(s, t) = \begin{cases} G_0 & \text{if } s(S, t) \in [\ell(t) - \ell_g, \ell(t)] \\ 0 & \text{otherwise,} \end{cases} \tag{1}$$

$$\partial_t \partial_S s(S, t) = G(S, t) \cdot \partial_S s(S, t),$$

where ∂_t denotes the partial derivative with respect to t. This law describes the primary extension process and we refer to G_0 as the extension parameter.

We now introduce the equations which characterize the sensing activity of the plant. The equation that we use is strongly related to the one described in [21] for growing trees. For modelling growing trees, the fundamental assumption is that the new layer of material formed during the secondary growth process do not affect the balance of the total forces and momenta which were previously applied to the stem [32]. Using a formal mathematical description, this means that the infinitesimal mass accretion due to secondary growth affects the intrinsic curvature κ, but not the current curvature $\partial_s \theta$. Here, we have used the term "intrinsic curvature" to denote the curvature of the intrinsic configuration and we have used the term "current curvature" to denote the curvature of the current configuration. The mathematical relation capturing how new layers affect the tree shape is provided by the equation [21]

$$\partial_t \kappa = -\frac{\partial_t B}{B}(\kappa - \partial_s \theta), \tag{2}$$

where $B(s, t)$ is the flexural rigidity of the rod at $r(S, t)$.

By also taking into account the effect of the tropisms and of the proprioception [21, 16], we obtain the following equation for the development in time of κ:

$$\partial_t \kappa = \frac{G v_R}{R^2}(\alpha \cos \theta - \beta \sin \theta) - G \gamma \partial_s \theta - \delta \frac{\partial_t B}{B}(\kappa - \partial_s \theta). \tag{3}$$

7

Here, the parameters α and β represent the response to a directional stimulus, while γ represents the sensitivity with respect to the proprioception. We will refer to them as *sensing* parameters. δ is the parameter regulating the intensity of the radial expansion effect on the shoot development. R is the radius of the circular cross section and v_R is the radial expansion rate. Similarly to what was done in the work by Bastien et al. [33], the dependence on the radius (and in our case, also on the radius expansion rate) is only on the term $\alpha \sin \theta - \beta \sin \theta$.

We now consider the effect of the elasticity on the climbing plant shoot development. The usual fundamental assumption is the following: the elastic equilibrium time scale is much shorter than the growth time scale [19]. In other words, the interval of time that the climbing plant shoot takes to reach the elastic equilibrium is not sufficiently long to observe any change in the climbing plant shoot total length or in the secondary growth. Such a modelling assumption justifies the use of elastic equilibrium theory for filaments shapes (see **S1** for further details). To compute the total force at a point of an elastic rod under the sole effect of gravity, one needs to know the total weight applied at that point. We refer to the term *linear density* ρ as the amount of mass per unit of length, while we refer to *volume density* ρ_3 as the amount of mass per unit of volume. So, the total weight of a shoot can be obtained by integrating the linear density of the main stem on $[0, \ell(t)]$ and by adding the leaves mass m_l, which vary both in time and in space along the stem. These considerations lead to the following relation:

$$\left[\int_s^{\ell(t)} \rho(\sigma, t) d\sigma + m_l(s, t) \right] g \sin \theta(s, t) = \partial_s[B(s, t)(\kappa(s, t) - \partial_s\theta(s, t))], \quad (4)$$

where $m_l(s, t)$ is the leaves mass from the apex to the point $s \in [0, \ell(t)]$ and g is the gravitational acceleration constant. One can observe that in equation (3) the current curvature $\partial_s\theta(s, t)$ affects the intrinsic curvature $\kappa(s, t)$ through the proprioceptive term, but the latter is different from the former. In the weightless case (that is, when the left hand side of equation (4) is constantly vanishing), the climbing plant weight no longer influences the climbing plant development, which is then fully described by the sensing equation (3), with $\kappa = \partial_s\theta$.

We now introduce a further equation connected with the variability of the linear density ρ, which is related with the flexural rigidity B. Naming E the Young's modulus, by definition of flexural rigidity we have $B(s, t) = EI(s, t)$, where $I(s, t)$ is the second moment of area at $s \in [0, \ell(t)]$ and at time t. Notice that, if we assume that the climbing plant shoot has a circular cross section of radius $R(s, t)$, the second moment of area is $I = \frac{\pi}{4}(R(s, t))^4$ and the volume density $\rho_3(s, t)$ is related with the linear density $\rho(s, t)$ via the equality $\rho(s, t) = \rho_3(s, t)\pi(R(s, t))^2$. This leads to the following formula, which expresses the proportionality between flexural rigidity and the square of the linear density:

$$B(s, t) = \frac{E}{4\rho_3(s, t)^2\pi}(\rho(s, t))^2. \quad (5)$$

2.2 Preliminary Simulations

As a preliminary step, we study the effects of variable density induced by the secondary growth on the model (1)-(5). For reasons of comparison with the models in the current literature, the development of the intrinsic curvature κ and the flexural rigidity B have the expressions displayed in equations (2.3) and (2.7) of [24]. The simulations that we run are set in different gravitropic sensitivity conditions and consider cases with constant density as well as cases with variable density. Since we want to compare the effect of the change in weight distribution, the total mass M is the same in each case. With the exception of the linear density distribution, all the remaining sensing and morphological parameters are arbitrarly chosen as displayed in table 1. The values for the linear density in the constant and in the variable cases were instead determined as follows. The variable density at each point of the stem is given according to (5) as $\rho = \sqrt{B/a}$, where a is a proportionality coefficient. On the other hand, we denote with ρ_c the linear density for the constant case. Since we want the plants to have the same total mass M at a certain time T (which is the same in all the simulations), we determine the values of a and ρ_c so that

$$M = \int_0^{\ell(T)} \sqrt{\frac{B(\sigma, T)}{a}} d\sigma = \ell(T)\rho_c, \tag{6}$$

where $\ell(T)$ is the length of a plant stem at time T which grows following the equations (1) with the parameters in table 1. To improve the comparison between the constant density case and the variable one, in addition to ρ_c we chose further values for the the constant density between $\rho_0 = \sqrt{B_0/a}$ and ρ_c. Comparing the shapes and comparing the evolution of height over time (see figure 2) it appears that a density distributed accordingly along the stem allows the plant to sustain a greater weight without sagging.

Parameter	Meaning	Value	Unit of Measure
G_0	Extension parameter	0.01	s^{-1}
ℓ_0	Initial length	0.1	m
ℓ_g	Extension zone	0.2	m
τ	Rigidification parameter	100	s
E	Young's modulus	10^7	$N \cdot m^{-2}$
r	Radius	$1 \cdot 10^{-3}$	m
I	Second moment of inertia	$\frac{\pi \cdot r^4}{4}$	m^4
B_0	Initial flexural rigidity	$E \cdot I$	$N \cdot m^2$
B_{max}	Maximal flexural rigidity	$10 \cdot B_0$	$N \cdot m^2$
g	Gravitation acceleration	9.81	$m \cdot s^{-2}$
γ	Proprioception	1	$Scalar$

Table 1: Parameters used for the preliminary simulations. The reference model is the one developed in [24], from which some of these parameters are taken.

(a) $\beta = 1$

(b) $\beta = 5$

(c) $\beta = 1$
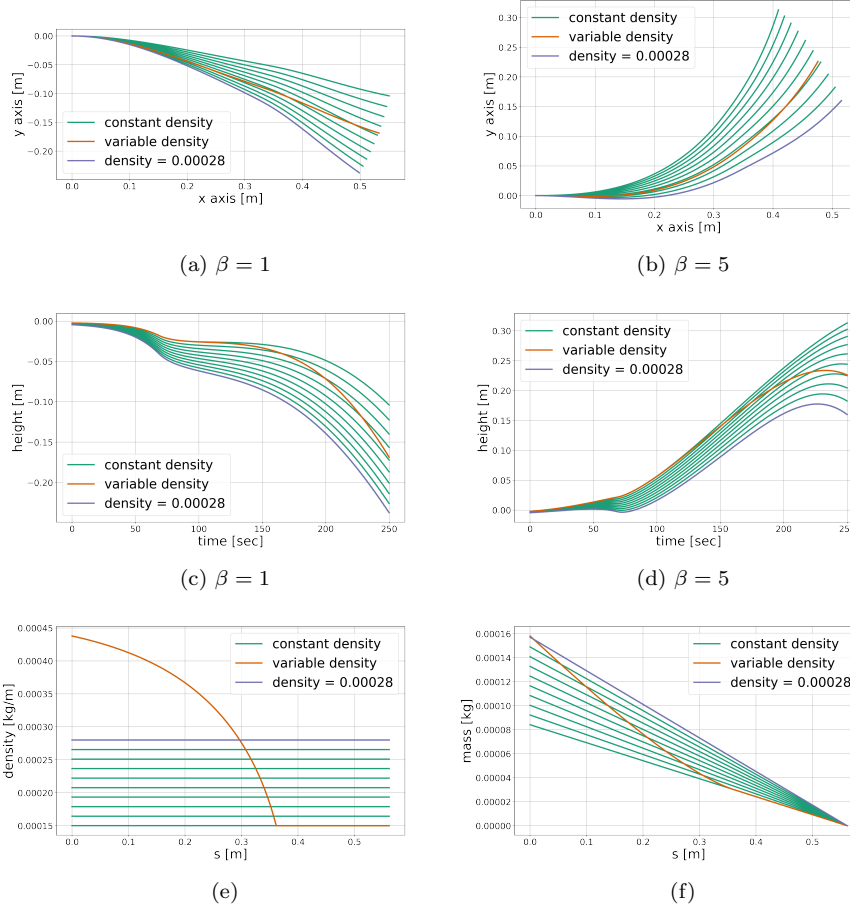
(d) $\beta = 5$

(e)

(f)

Figure 2: Comparisons between constant and variable density in an artificial environment. Figures 2a, 2b represent the simulations of the searcher shoot with different distributions of the linear density for two graviceptive parameters: $\beta = 1$ and $\beta = 5$. The green lines and the violet line stand for the final stage of the simulations for searcher shoots with constant linear density, whose values correspond to the green lines and the violet line in figure 2e. In that figure, the abscissas are the distance from the base (in m), while the ordinates are the linear density (in $kg \cdot m^{-1}$). The orange line in figures 2a, 2b is the final stage of a simulation with a variable linear density. The distribution of the linear density along the shoot is displayed by the orange line of figure 2e. Figures 2d, 2c represents the height reached by the simulated stems respectively of figures 2a and 2b in function of time. Figure 2f represents the mass of the portion of the shoot whose points are at least s meters from the base. So, for $s = 0$ we have the mass of the whole shoot. As we can observe, the shoot with the variable linear density is bearing the highest amount of mass; nevertheless, it is able to bear its own weight, unlike most stems with the constant linear density which droops under the effect of gravity.

2.3 Application to Real Plants and Simulations

The above arguments encouraged the use of a variable linear density term, and consequently a model which takes the secondary growth into account, to attempt simulations based on experimental data from climbing plants. In the following sections we show the application of our model to two climbing plant species, *T. jasminoïdes* and *C. guianense*. The analysis includes experimental data on representative characteristics of each searcher shoot including geometry, mechanics and growth. These data were then used to calibrate the morphological parameters of the model (see table 2).

Parameter	Value	Value	Unit of Measure
	T. jasminoïdes	*C. guianense*	
G_0	0.15	0.12	day^{-1}
ℓ_g	0.14	0.17	m
a_{fr}	0.016	0.28	$Kg\, m^3 day^{-1}$
b_{fr}	4.18	4.11	m^{-1}
c_{fr}	0.69	1.58	m
a_l	$5.7 \cdot 10^{-5}$	0.006	kg
b_l	10	5.67	m^{-1}
c_l	0.1	1.15	m

Table 2: Parameters for extension, flexural rigidity, volume density and linear density of leaves for *T. jasminoïdes* and *C. guianense*. These parameters refer to the equations of the model described in section 2.1. The extension parameters G_0 and ℓ_g have been retrieved by averaging the measurements on the elongation of the internodes in various samples of the two species. Instead, the other parameters are the result of a fitting operation with the experimental data.

Parameters involved in sensing, i.e. α, β and γ, were estimated by using the quantitative information about the reach and the orientation of the plant at the final stage (see figure 1a and section 2.3.4 for further details about the method used to estimate them).

2.3.1 Geometry and Biomechanical Properties

In a first experiment, we collected morphological and biomechanical data from five searcher shoots for each species. For each individual, we selected, as far as possible, the longest searcher shoots in a self-supporting state. In their natural position, we measured the reach (cm) and orientation (degrees from the horizontal) defined as a straight line from the base to the apex of the searcher shoot. The geometry of the shoot was described from internodes of the main stem. For each successive internode, we measured its length and its median diameter obtained from the mean of two orthogonal measurements. Bending properties of the base of the searcher stem were measured using four-point bending tests on a stem segment constituted of several internodes [34]. Flexural rigidity EI and structural Young's modulus E_{str} were calculated from applied bending forces

plotted against maximum deflections. Up to five weights were applied manually and each deflection was measured by observation with a dissecting microscope on the apparatus. Weight increments were chosen according to the bending resistance of each sample. Weights were constituted of stainless-steel or brass ranging from $8\,g$ (*C. guianense*) to $50\,g$ (*T. jasminoïdes*). Span distances were defined as proportional to the mean elliptical diameter of the stem segment. The span support was 40 times greater than the diameter and was ranging from $107\,mm$ to $218\,mm$ for the longest. The load span was comprised between one half and two thirds of the span support and ranged from $67\,mm$ to $120\,mm$. In four-point bending, the flexural rigidity EI ($N\,mm^2$) was calculated via the following formula:

$$a = \frac{L - l}{2},$$

$$EI_{4\mathrm{pt}} = b \cdot \frac{L^3}{48} \cdot \frac{3a}{L} - 4 \cdot \left(\frac{a}{L}\right)^3,$$

where l is the load support (i.e. the distance between two internal supports), L is the span support (i.e.the distance between the two outside panniers) and b is again the slope of the force-deflection curve (N/mm). For three positions along the measured segment (basal, medial, apical), the vertical diameter d_v was measured and the means then used to calculate the second moment of area I of the axis. Since measured shoots generally exhibited a slightly ellipsoidal cross-section, we used the following formula:

$$I_{ellipse} = \frac{\pi}{4} \cdot \left(\frac{d_v}{2}\right)^3 \cdot \frac{d_h}{2}.$$

However, the experimental measurements show that the difference between d_v and d_h is small, so it is reasonable to assume a circular cross section. The structural Young's modulus of the stem (E_{str}) (MN/m^2) was estimated with the following formula [35] :

$$E_{str} = EI/I.$$

2.3.2   Extension Parameters: rate and zone

Primary growth, is generally viewed as axial stem extension, resulting from the coordinated activities of three meristematic regions at the shoot apex [36, 37]. The first region, known as shoot apical meristem, is the position of intense cell division initiating the differentiation between nodes and internodes that constitute the stem. The second one, known as rib meristem, leads to the formation and differentiation of primary tissues such as the pith. Meanwhile the third region, named intercalary meristems, is located at the bases of one or several apical internodes and their elongation also result in the axial extension of the stem. During stem extension, several successive internodes may elongate simultaneously up to their final length. To describe these processes in the simplest form, we considered two parameters (see figure 3):
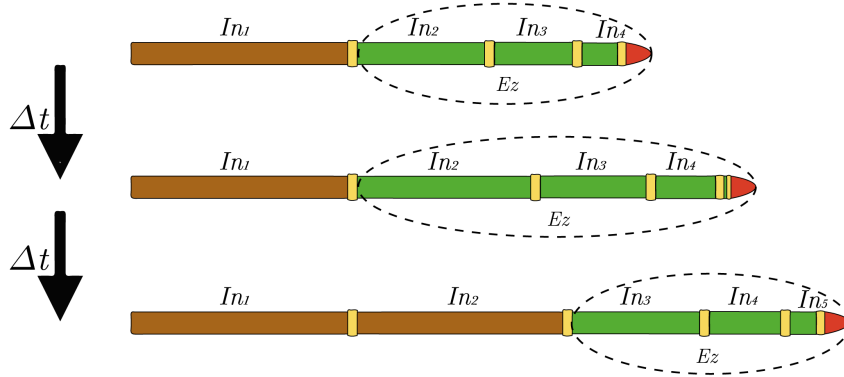
Figure 3: Extension of the internodes. The figure represents the main stem of a searcher shoot divided into internodes and the apical-most segment (red). After one of time Δt, the combined length of the green internodes and the total length has changed, whereas the length the brown ones has not. After a second period Δt, the longest green internode (In_2) has reached its maximal length and has stopped elongating. This latest green segment can now be considered mature and outside of the extension zone and is thus depicted as brown in the second Δt time frame. The sum of the green internode lengths gives an approximation of the length of the extension zone of the shoot at a given time interval.

- the extension rate $\dot{\ell}(t)$, which corresponds to the speed of extension at the stem level;

- the extension zone, that is the apical elongation portion of the stem (also called growth zone [27]). The length of the extension zone is connected with the parameter ℓ_g displayed in equation (1).

To calibrate these parameters, we monitored the extensional growth of young, self-supporting, searcher shoots over one week for 11 shoots of *T. jasminoïdes* and one month for 19 shoots of *C. guianense* (see section *Materials and Methods* in [29] for further information on the environmental conditions). Three dates at three days interval have been recorded for *T. jasminoïdes* and five dates at 7 days of interval for *C. guianense*. For both species, we applied the same protocol starting by defining a reference mark on the most basal node of each main stem. From this mark, we measured at each date:

- the total length of the shoot (cm);

- the length of each successive internode up to and including the apex (cm).

Between each time interval, the difference in total length of the stem allowed us to estimate an extension rate $\dot{\ell}(t)$, expressed in cm/day. The natural organisation of the shoot into separate internodes allowed us to identify and measure

13

which internodes elongated between two dates. The sum of the internodes length was used to estimate the length of the extension zone in cm for each time interval.

Successively, we used these estimates to compute the parameters ℓ_g and G_0 of the model. According to the model, the parameter ℓ_g for a shoot represents the maximal length value of its the extension zone. At the beginning of its development, the whole shoot is elongating, so at this moment the length of the extension zone actually represents the length of the whole stem. Hence, we could estimate the value of ℓ_g only for the shoots whose length of the estimated extension zone was lower than the length of the whole stem. For these cases, ℓ_g coincides exactly with the length of the extension zone.

Since many random effects that may have influenced the shoot extension over these periods (e.g. local light, temperature, herbivores, support finding, etc.), we decided to compute a single value of ℓ_g for all the shoots of the same species. To do so, we took the average over all the estimated ℓ_g. We proceeded in a similar way for the estimate of G_0. For the shoots whose extension zone is shorter than the whole stem, the model predicts a linear growth regime. This means that for these cases, the extension rate is constantly $\dot{\ell}(t) = \ell_g G_0$. So, G_0 has been estimated as the average of the ratio $\dot{\ell}(t)/\ell_g$.

2.3.3 Experimental Data Fitting

The data provided by the first experiment explained in section 2.3.1 were used for the fitting procedure of volume density ρ_3, radius R, radial expansion speed v_R, flexural rigidity B and leaves mass m_l. This fitting procedure was specific for each shoot, that is, for each shoot we retrieved the parameters of the above-mentioned functions. To obtain a spatio-temporal information from a static description of the shoot, we assume that at a given distance from the tip, all the properties of the shoot do not change in time. This seems to be reasonable, since the primary growth takes place at the shoot apex and the further a stem portion is positioned away from the tip, the more it has matured. So, consider for instance the volume density ρ_3 for a given shoot. The experimental data has been taken at a fixed time of the evolution of that shoot and, for this reason, they are a static description of it. However, we know the total length of the shoot and the positions at which the volume density was measured, so we can put ρ_3 in function of the distance from the tip. By our assumption, now we can compute the volume density at each time t and at each position $\mathbf{r}(s, t)$ by considering the quantity

$$\rho_3(\ell(t) - s)$$

because the difference $\ell(t) - s$ provides exactly the distance of the point $\mathbf{r}(s, t)$ from the shoot tip.

We fitted the data ρ_3, R and v_R with a second degree polynomial in function of the distance from the tip. On the other hand, we assumed the biomass accretion of a single leaf $\hat{m}_l$ behaves according to the following equation

$$\hat{m}_l(s, t) = \frac{a_l}{1 + \exp(b_l \cdot (c_l - (\ell(t) - s)))}, \tag{7}$$

14

where a_l, b_l, c_l are fitting parameters to be tuned in accordance to the leaves mass measurements. The function $m_l(s,t)$ introduced in equation (4) is the total mass of the leaves which affect the point $\mathbf{r}(s,t)$. To retrieve m_l from $\hat{m}_l$, it is sufficient to sum the single leaf masses at the internode basis whose arc length is grater than s. If, for each time t, we use $s_i(t)$ to denote the arc length of all the internode basis, and $n_i^l(t)$ to denote the corresponding number of leaves (here i varies form 1 to the total number of internodes), then we can write

$$m_l(s,t) = \sum_{\{i\,:\,s_i(t)\geq s\}} n_i^l(t) \cdot \hat{m}_l(s_i(t),t).$$

The choice of a sigmoid for fitting the mass distribution of a leaf is due to the fact that leaf life cycle is much shorter than the climbing plant shoot life cycle. Consequently, at the base of the shoot we can find the oldest leaves, which are close to a final mature state, while at the shoot apex there are very few leaves. Leaf behaviour during the life cycle can be interpreted well as a sigmoid function, which can be close to zero ate the apex, is monotonically increasing as a function of the distance from the apex and, finally, approaches a saturation value at the base.

Since the estimates of the flexural rigidity $B(s,t)$ at the internode basis for different shoot samples show a monotonically increasing behaviour with respect to the distance from the the apex, we also used a sigmoid to obtain an approximation of B at every point $s \in [0,\ell(t)]$ and every time t:

$$B(s,t) = \frac{a_{fr}}{1 + \exp(b_{fr} \cdot (c_{fr} - (\ell(t) - s)))},$$

where a_{fr}, b_{fr}, c_{fr} are fitting parameters to be tuned.

As for the computation of the volume density from the experimental data, we considered the fresh cylindrical volume and the fresh mass of each internode, obtained from the measured length and orthogonal diameters. The experimental data indicated that the horizontal and the vertical diameters have approximately the same values, justifying the modelling of the shoot with a circular cross-section. To compute the radial expansion speed v_R, we included the increase in the radius for each internode and divided it by the extension rate $\ell_g G_0$. More precisely, if s_i and s_{i+1} are the basis arch length of two consecutive internodes with $s_{i+1} > s_i$, then

$$v_R(s_i) = \frac{R(s_i) - R(s_{i+1})}{\ell_g G_0}.$$

In this way, we obtain an estimate of the radial expansion speed for each internode. For the computation of the flexural rigidity B, we extrapolated the second moment of area I at the base of each internode. For the Young's modulus E, in this investigation, as a first approximation, we assumed it as a constant along the whole searcher stem, with constant value based on the measurement at the base of the shoot. Previous studies and tissue organisations along searcher shoots indicate that E diminishes towards the apex of searcher shoots [3, 38] so the values used in this study are an approximation. Finally, for the second moment of area, we used again the orthogonal diameters of the cross-section.

2.3.4 Simulations

In the previous sections we have explained how we retrieved the average extension parameters, G_0 and ℓ_g, and the shoot-specific parameters for equations (3)-(7), from measurements based on living *T. jasminoïdes* and *C. guianense* plants. Simulations for these cases (see figure 4) were set up with an initial length equal to ℓ_g. In this way, the growth regime is linear and the time interval $[0, T]$ for a simulation can easily be retrieved from the final length of the shoot ℓ_f with the ratio $T = \frac{\ell_f - \ell_g}{\ell_g G_0}$. Using the information about the reach and the orientation, we were able to estimate the sensing parameters α, β and γ. To this aim, we used the numerical function `minimize` of the library `SciPy` in `Python` to choose the set (α, β, γ) which minimised the squared difference between the simulated and the experimental reach and orientation.

In a first set of simulations, we set the parameter δ equal to 0. Succesively, to study the effects of the radial expansion term on the shoot development, we set different values as described in Figure 6.

Given the lack of variety of data and considering that the plant samples were taken in an uncontrolled environment, these estimates can certainly be improved by further measurements and experiments. However, we think that these estimated values are sufficiently accurate to realistically simulate the observed behaviours and to represent the model.

3   Results

The simulations that we obtained using the radial expansion parameter $\delta = 0$ and the parameters estimated from the experimental data are displayed in Figure 4. For *T. Jasminoïdes*, the initial inclination of the stem with respect to the vertical line is $\pi/4$ radians. Initially the stem grows upwards, but it is clear from the changes in the inclination of the tip that the growth direction is changing. Soon, the apical part of the shoot starts growing downwards.

The case of *C. guianense* is different. The simulation displays a strong horizontal extension of the shoot. The initial inclination of the main stem is $\pi/2$ radians with respect to the vertical line, which means that, at the beginning, the shoot is directed horizontally. Looking at the time evolution displayed in Figure 4, we see that the tip is directed upward. Nevertheless, it is clear that in the simulation the whole *C. guianense* stem is drooping due to its weight.

Finally, considering again the model described by equation (1)-(3)-(4)-(5), we fixed different values of δ and calibrated again the sensing parameters (α, β, γ) as described in section 2.3.4. The parameters G_0, ℓ_g, R and v_R are based on the *C. guianense* dataset. The resulting simulations for different values of δ are displayed in Figure 6, in which we can observe an increasing curling behaviour of the apex as δ increases.
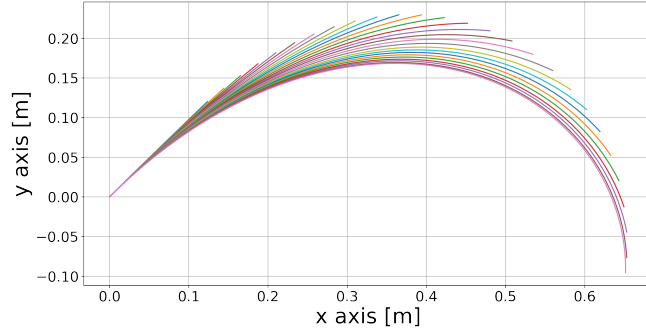
(a)
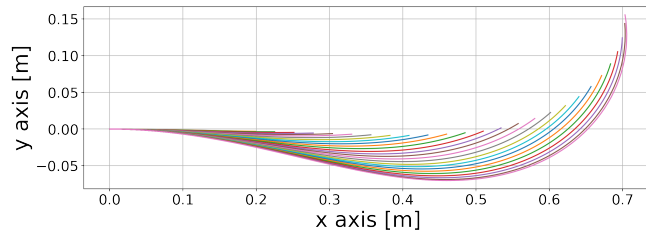
(b)

(c)

(d)

Figure 4: (4b),(4a): Simulations for *T. jasminoïdes* and *C. guianense*, respectively. The axes represent the (x, y)-coordinates of the simulation in the plane; the different colours represent the different time steps of the simulation; each line of a single colour stands for the main stem. Each stem has a fixed origin point at (0,0). The simulation of *T. jasminoïdes* has an initial inclination of $\pi/4$ with respect to the vertical line, while that of *C. guianense* has a horizontal initial inclination. In both cases the plant develops horizontally. The behaviour of the *T. jasminoïdes* is due to its sensing activity, which displays a negative parameter β. In contrast, that of *C. guianense* droops because of its weight.

(4c),(4d):Images of *T. jasminoïdes* and *C. guianense*, respectively, in their natural habitat. As one can observe, they resemble the simulations: the *T. jasminoïdes* curls around towards itself, growing downwards; the *C. guianense* is strongly horizontally directed and points upwards with its tip.

17
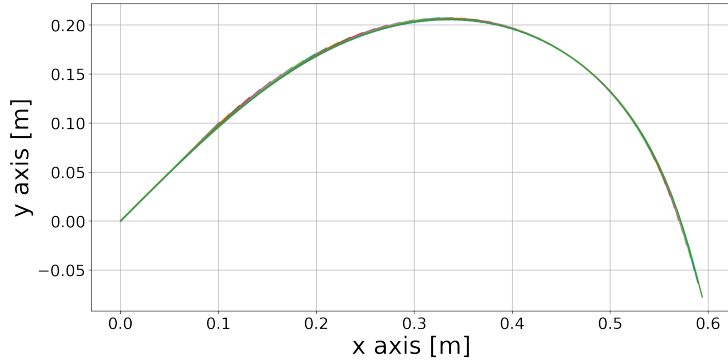
(a)
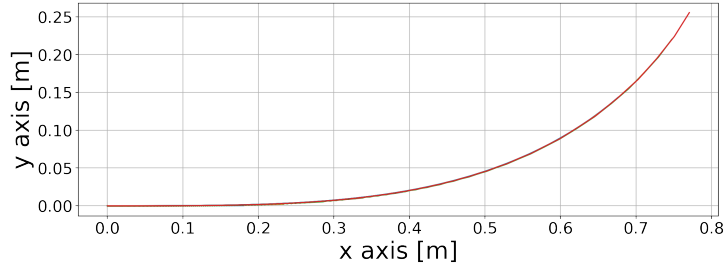
(b)

Figure 5: Simulations for *T. jasminoïdes* and *C. guianense* respectively. These simulations are based just on the growth equation (1) and equation (8), that is, they neglect the mechanics. The sensing parameters (α, β, γ) are optimised to obtain the best reach and orientation according to the experimental data. We can observe that the simulation 5a for the *T. jasminoïdes* is growing downwards. The displayed behaviour is due to the sensing activity, in accordance with the result obtained for the simulation of the *T. jasminoïdes* in figure 4a.

On the other hand, the *C. guianense* is just growing upwards, differently from figure 4b. This means that the mass can play a fundamental role in the formation of the plant shape.

4 Discussion

4.1 Interpretation and limitaitons of the result

The model developed in this study combines the primary growth of a searcher shoot (i.e. tip growth inducing stem extension) with the postural responses incorporating lateral expansion of the stem (i.e. secondary growth of the wood cylinder and maturation of primary tissues). These processes have been complemented by the variation of stem flexural rigidity EI (expressed by the function B in equation (4)) and trough the time development of the intrinsic curvature κ. As displayed in section 2.3.1, the flexural rigidity was calibrated from the values of the (structural) Young's modulus E observed at the base of the shoot, and from the series of diameters measured along the shoot to estimate the second moment of area I. In this procedure, E is considered to be constant in time and space. This simplification does not take into account the variations in E that may exist due to the non-homogeneous tapering of tissues in the stem and their maturation. Although the variations along the climbing plant shoot of Young's Modulus and second moment of area can well be of the same order, the variation of R plays a major role in the displayed simulations since it appears at the denominator of the sensing parameters in equation (3). Furthermore, the choice of $\delta \approx 0$ in the simulations mitigates the effect of the Young's Modulus variation (which affects merely the flexural rigidity appearing in equation (3)) along the climbing plant shoot.

In the simulations displayed in Figure 4b-4a, we observed that the stem is sagging. However, looking at the sensing parameters obtained in the fitting procedure (see Table 3), we were able to distinguish whether the behaviour is due to the sensing activity of the shoot or ot its weight. The negative β for the *T. jasminoïdes* expresses a downward stimulus which causes a downward growth. So, we could conclude that the main driver of the *T. jsaminoïdes* behaviour is the sensing activity. On the other hand, applying the same reasoning to the *C. guianense* stem, we reached the opposite conclusion. The positive β denotes a preference for an upward growth, which explains the behaviour of the tip. However, as a consequence of its own weight, the main stem has a mostly horizontal development with a steep vertical change of growth in the part of the stem close to the tip.

Another evidence of the distinct role of the weight distribution along the stem in *T. jasminoïdes* and *C. guianense* behaviours is provided by the outcome of the simulations of the "weightless model" based just on the growing equation (1) and on the following evolution equation of the curvature

$$\partial_t \kappa = \frac{Gv_R}{R^2}(\alpha \cos\theta - \beta \sin\theta) - G\gamma\kappa. \tag{8}$$

Again, we can extrapolate G_0, ℓ_g, R and v_R from the experimental data, calibrate the sensing parameters (α, β, γ) from the reach and the orientation of the shoot in consideration and set all these values as parameters in the equation (1) and in equation (8). The resulting simulations are displayed in figure 5. A com-

	T. jasminoïdes	*C. guianense*	Unit of Measure
α	0.0005	0.001	*day*
β	-0.005	0.004	*day*
γ	0.008	0.004	*scalar*
α	0.0068	0.0025	*day*
β	-0.003	0.002	*day*
γ	0.02	0.02	*scalar*

Table 3: Sensing parameters used for the numerical simulations. In the upper side of the table, there are the values used for figures 4, while at the bottom there are the values for the case without the mechanics displayed in figure 5. All these parameters have been optimised to best fit the experimental reach and orientation.

parison between the two sets of simulations confirm the results on the role of the weight distribution along the shoots previously exposed. Indeed, as we can see in table 3, the sensing parameter β for the weightless *T. jasminoïdes* is negative and the sensing activity orients the tip shoot downwards in a way similar (but not equal) to the case in which the weight affects the plant shoot development. On the other hand, the weightless *C. guianense* immediately grows upwards, without displaying a horizontal structure in the shoot portion before the apex.

4.2 The role of the radial expansion parameter δ

In the study by Guillon et al. [21], it is assumed that the stem radial accretion does not change the local current curvature (see, e.g., the simulations in Figure 6 and related caption). Such an assumption led Guillon et al. to adding the term

$$\frac{\partial_t B}{B}(\partial_s \theta - \kappa) \tag{9}$$

in the sensing equation. The tendency to maintain the local current curvature rather than straighten the stem is in contrast with the stem is in contrast with the stem proprioceptive activity. From a mathematical point of view, we can observe that the term $\frac{\partial_t B}{B}\partial_s \theta$ appearing in equation (3) has an opposite sign with respect to the proprioceptive term, acting like a "negative proprioception" term in the sensing equation. Indeed, the ratio $\frac{\partial_t B}{B}$ is non-negative since the flexural rigidity B is both positive and increasing in time. Hence, if we consider the equation (3) with $\delta > 0$, it follows that the term $\delta \frac{\partial_t B}{B}\partial_s \theta$ has an opposite sign with respect to the proprioceptive term $-G\gamma\partial\theta$. In particular, this means that the term $\frac{\partial_t B}{B}\partial_s \theta$ can mitigate (or destroy) the strightening effect of the proprioceptive term, introduced in [16] exactly to stabilize the sensing equation.

The occourence of a "negative proprioception" is shown in the simulations in Figure 6, in which we can observe that the curling behaviour of the tip increases as the parameter δ increases. In particular, this behaviour affects the elongation direction of the tip, which grows downwards when it starts curling and then grows upwards again, resembling the gravitropic "sign reversal" displayed in [24].
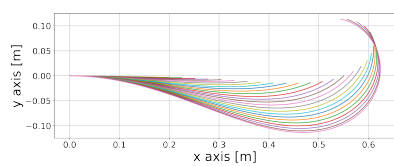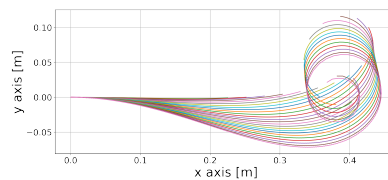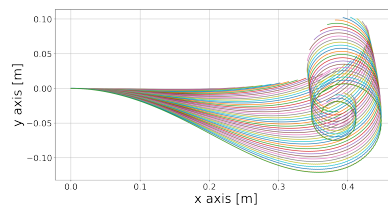
(a) $\delta = 0.25$ (b) $\delta = 0.5$
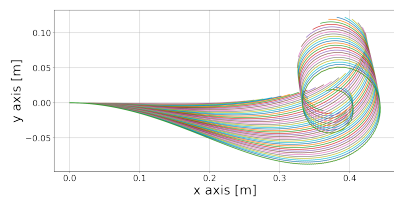
(c) $\delta = 0.75$ (d) $\delta = 1$

Figure 6: Simulations of *C. guianense* for increasing values of δ. Each of these simulations are obtained by following the procedure described in section 2.3, so the sensing parameters are optimized to meet the experimental reach and orientation and may change among the simulations. We can observe the effect of the "negative proprioceptive" term $(\partial_t B/B)\partial_s \theta$ which amplifies the curling behaviour of the tip. This curling effect resembles the gravitropic "sign reversal" displayed in [24].

4.3 Biological interpretations

The application of the 2D-model with $\delta \approx 0$ and calibrated with field data showed that a full description of primary and secondary growth processes as well as a description of the sensing activity were fundamental to reproduce self-supporting growth of searcher shoots. Numerical simulations were able to reproduce similar maximal reach capacities as those observed in the field for both species. Simulations showed that both species exhibited horizontal trajectories of self-supporting growth to attain their maximal reach capacities. 2D postures obtained at the end of the simulations were qualitatively equivalent to the ones observed in the field. Both species expressed a self-weight movement induced by mass distribution (in space) and accretion (in time). Nevertheless, they differed in terms of postural dynamics. These differences can be interpreted numerically by both sensing and mechanical parameters. From a sensing point of view, *C. guianense* exhibited a stronger anti-gravitropic and autotropic behaviour than *T. jasminoïdes*. These explain the apical orientation of searcher shoots leading to an upward growth for *C. guianense* and a downward growth for *T. jasminoïdes*. From a mechanical point of view, *C. guianense* was more strongly effected than *T. jasminoïdes* in maintaining an upward growth in view of a faster mass accretion along the searcher shoot. However, these biological interpretations must be interpreted with caution with respect to the size of the dataset and observations that have been made under natural conditions without control over external factors.

4.4 Future Improvements

The model developed here provides a theoretical and analytical framework that can be a useful tool to better understand the strategies of lianas to cross gaps with their searcher shoots under the effects of gravitational constraints. In particular, it allows us to see how the mass distribution, the stiffness and the length of the shoot influence its development and space orientation. To this purpose, the model parameters are fitted with the experimental data. As displayed in section 3, for the *T. jasminoïdes* case this fitting procedure returns a negative parameter β, which is related to the vertical direction of the stimuli response activity. Since the climbing plant samples were not raised in a controlled environment, we cannot immediately interpret the negative value of β and the related behaviour of the simulation (Figure 4b) with a positive gravitropic behaviour. Nevertheless, the relation between the values of the sensing parameters and the observed behaviour of the climbing plant under unpredictable environmental conditions can be a matter of further studies.

Despite the uncontrolled environment and the basic measurements based on fully elongated shoots, the 2D-model revealed to be robust enough to reproduce the self-supporting state of the climbing plant species considered in this work. Moreover, the model can already take into account the tissue anatomical variations along the stems in terms of flexural rigidity, mass and radius, and how such variations affect the final climbing plant shape. Moving in the direction

of a more in-depth study of the shoot structure, it may be interesting to investigate how the biomechanical state and biomass allocation changes during the extension of a searcher shoot form a dynamic point of view. This would imply working on a large set of searcher shoots, regularly sacrificing some of them for destructive measurements, and reasoning in terms of chronosequence (i.e. by extrapolation), trying to work under conditions that are as homogeneous as possible in order to minimize the uncertainty factors (ontogenetic stage, environment, etc.). These measurements associated with the anatomical study of the tissues could allow a better understanding of the mechanism at the origin of the rigidification dynamics at all points of the searcher shoots. The anatomical organizations in the mechanical and postural life-histories of plant is a promising scientific research to conceal ecology, biomechanics and robotics [39].

Searcher shoots are highly diverse in climbing plants and can have relatively complex structures depending on types of connected structures such as leaves, hooks, tendrils, branches, stem segments capable of circumnutatory movements, as well as intrinsic stem extension and postural dynamics [29]. The movements associated with these structures and generated by growth differentials within tissues are of significant importance for exploring and crossing spaces and attaching to supports. The model considered here in 2D is relatively simple and corresponds to an unbranched shoot with differential dynamics between internodes and leaves. The consideration of a more complex shoot structures, involving variable mass load distributions in space an time and in a 3D volume is a higher step to properly simulate the self-supporting and searching mobility of searcher shoots in climbing plants. For instance, a 3D version of the model presented in this paper could be used to understand the role of circumnutation in climbing plant searching strategy. Another possible application of a 3D model could be to study how climbing plants change their mechanical internal properties when they encounter external obstacles which they attach to. All these problems cannot be addressed by using a 2D model and will be the subject of future studies.

4.5   Conclusion

We formulated a model that takes secondary growth and proprioception into account. Through preliminary simulations, we showed how variability in linear density induced by the radius expansion can affect the capability of a plant to sustain its own weight. We then showed how it is possible to estimate the parameters of the model from the experimental data. Using the information about the extension of the stem, we computed the extension parameter G_0 and the length of the extension zone ℓ_g. Then, based on experimental data on the final reach and orientation of each stem, we calibrated the sensing parameters α, β and γ. Based on such measurements and on the related simulations in Figure 4a-4b, we were able to understand the role of the weight in the shapes observed in Figure 4c-4d.

For the two cases in exam, we were able to say that the mechanical effect of the weight plays an important role in the shape of the *C. guianense*, while

the downward growth of the *T. jasminoides* is mainly the consequence of its sensing activity. These conclusions are supported by the simulations based on a simplified model which considers just the plant sensing activity (see figure 5). Such results confirm that the mechanical aspects in climbing plant searcher shoots, and, in particular the variable linear density and the secondary growth are not negligible in order to obtain realistic climbing plant shapes in experimental data-based simulations.

Supporting information

S1 text. Appendix. Derivation of the analytical and numerical model. Spectral analysis of the gravi-proprioceptive model. Figure (S1a-S1b-S1c): Simulations of system (S10). The parameter β is set to the value 10 in all the simulations, the arc length parameter S belongs to $[0,1]$ and the time t is in $[0,2]$. We can observe that the oscillations of the shoot increases as the parameter γ decreases. Figure (S1d): the eigenvalues for the linear operator in system (S11). In green, the eigenvalues for $\gamma > 0$, in red for $\gamma < 0$ and in blue for $\gamma = 0$. We observe that some eigenvalues of the case $\gamma > 0$ has positive real part, denoting that the equilibrium $(\theta, \kappa) \equiv (0,0)$ is not stable.
(PDF)
S2. Table. Experimental morphological data. (.csv)
S3. Table. Experimental growth data. (.csv)
S4. Code. Code used for the simulations. (.py)

Funding

Acknowledgements

Author's Contribution

Michele Palladino and Fabio Tedone conceived of the presented idea. Michele Palladino and Giacomo Vecchiato developed the theoretical formalism. Giacomo Vecchiato planned and carried out the simulations with the help of Fabio Tedone and he wrote the manuscript with the help of Michele Palladino and Tom Hattermann. Tom Hattermann collected the experimental data with the supervision of Patrick Heuret and Nick Rowe. Patrick Heuret and Nick Rowe critically revised the manuscript, giving fundamental biological insights. Pierangelo Marcati supervised the project, providing critical feedback. Nicholas P. Rowe and

References

[1] Ernesto Gianoli. "The behavioural ecology of climbing plants". In: *AoB plants* 7 (2015).

[2] Nicholas P. Rowe, Sandrine Isnard, and Thomas Speck. "Diversity of mechanical architectures in climbing plants: an evolutionary perspective". In: *Journal of Plant Growth Regulation* 23.2 (2004), pp. 108–128.

[3] Nicholas P. Rowe and Thomas Speck. "Biomechanical characteristics of the ontogeny and growth habit of the tropical liana Condylocarpon guianense (Apocynaceae)". In: *International Journal of Plant Sciences* 157.4 (1996), pp. 406–417.

[4] Guy Caballé. "Le port autoportant des lianes tropicales: une synthèse des stratégies de croissance". In: *Canadian Journal of Botany* 76.10 (1998), pp. 1703–1716.

[5] Mariane S Sousa-Baena, José Hernandes-Lopes, and Marie-Anne Van Sluys. "Reaching the top through a tortuous path: helical growth in climbing plants". In: *Current Opinion in Plant Biology* 59 (2021), p. 101982.

[6] Charles Darwin and Francis Darwin. *The power of movement in plants.* John Murray, 1880.

[7] Moritaka Nakamura, Takeshi Nishimura, and Miyo Terao Morita. "Gravity sensing and signal conversion in plant gravitropism". In: *Journal of experimental botany* 70.14 (2019), pp. 3495–3506.

[8] Simon Gilroy. "Plant tropisms". In: *Current Biology* 18.7 (2008), R275–R277.

[9] Masatoshi Taniguchi et al. "The Arabidopsis LAZY1 family plays a key role in gravity signaling within statocytes and in branch angle control of roots and shoots". In: *The Plant Cell* 29.8 (2017), pp. 1984–1999.

[10] Miyo Terao Morita. "Directional gravity sensing in gravitropism". In: *Annual review of plant biology* 61 (2010), pp. 705–720.

[11] Daniele Agostinelli, Antonio DeSimone, and Giovanni Noselli. "Nutations in plant shoots: Endogenous and exogenous factors in the presence of mechanical deformations". In: *bioRxiv* (2020).

[12] Derek E Moulton, Hadrien Oliveri, and Alain Goriely. "Multiscale integration of environmental stimuli in plant tropism produces complex behaviors". In: *Proceedings of the National Academy of Sciences* (2020).

[13] Daniele Agostinelli et al. "Nutations in growing plant shoots: The role of elastic deformations due to gravity loading". In: *Journal of the Mechanics and Physics of Solids* 136 (2020), p. 103702.

[14] Hugo Chauvet et al. "Revealing the hierarchy of processes and time-scales that control the tropic response of shoots to gravi-stimulations". In: *Journal of Experimental Botany* 70.6 (2019), pp. 1955–1967.

[15] Julius Sachs. "Uber orthotrope und plagiotrope Pflanzenteile". In: *Arb Bot Inst Würzburg* 2 (1882), pp. 226–84.

[16] Renaud Bastien et al. "Unifying model of shoot gravitropism reveals proprioception as a central feature of posture control in plants". In: *Proceedings of the National Academy of Sciences* 110.2 (2013), pp. 755–760.

[17] DE Moulton, TH Lessinnes, and A Goriely. "Morphoelastic rods. Part I: A single growing elastic rod". In: *Journal of the Mechanics and Physics of Solids* 61.2 (2013), pp. 398–427.

[18] Raymond E Goldstein and Alain Goriely. "Dynamic buckling of morphoelastic filaments". In: *Physical Review E* 74.1 (2006), p. 010901.

[19] OM O'Reilly and TN Tresierras. "On the evolution of intrinsic curvature in rod-based models of growth in long slender plant stems". In: *International journal of solids and structures* 48.9 (2011), pp. 1239–1247.

[20] Hiroyuki Yamamoto, Masato Yoshida, and Takashi Okuyama. "Growth stress controls negative gravitropism in woody plant stems". In: *Planta* 216.2 (2002), pp. 280–292.

[21] Thomas Guillon, Yves Dumont, and Thierry Fourcaud. "A new mathematical framework for modelling the biomechanics of growing trees with rod theory". In: *Mathematical and Computer Modelling* 55.9-10 (2012), pp. 2061–2077.

[22] Tancrède Alméras and Meriem Fournier. "Biomechanical design and long-term stability of trees: morphological and wood traits involved in the balance between weight increase and the gravitropic reaction". In: *Journal of theoretical Biology* 256.3 (2009), pp. 370–381.

[23] Thierry Fourcaud et al. "Numerical modelling of shape regulation and growth stresses in trees". In: *Trees* 17.1 (2003), pp. 31–39.

[24] Raghunath Chelakkot and Lakshminarayanan Mahadevan. "On the growth and form of shoots". In: *Journal of The Royal Society Interface* 14.128 (2017), p. 20170001.

[25] Bruno Moulia et al. "The shaping of plant axes and crowns through tropisms and elasticity: an example of morphogenetic plasticity beyond the shoot apical meristem". In: *New Phytologist* 233.6 (2022), pp. 2354–2379.

[26] Bruno Moulia, Stéphane Douady, and Olivier Hamant. "Fluctuations shape plants through proprioception". In: *Science* 372.6540 (2021), eabc6868.

[27] Bruno Moulia et al. "Posture control in land plants: growth, position sensing, proprioception, balance, and elasticity". In: *Journal of Experimental Botany* 70.14 (2019), pp. 3467–3494.

[28] T Speck. "Bending stability of plant stems: ontogenetical, ecological, and phylogenetical aspects". In: *Biomimetics (USA)* (1994).

[29] Tom Hattermann et al. "Mind the Gap: Reach and Mechanical Diversity of Searcher Shoots in Climbing Plants". In: *Frontiers in Forests and Global Change* 5 (2022).

[30] Patricia Soffiatti et al. "Trellis-forming stems of a tropical liana Condylocarpon guianense (Apocynaceae): A plant-made safety net constructed by simple "start-stop" development". In: *Frontiers in Plant Science* 13 (2022).

[31] Benedikt Hoffmann et al. "Mechanical, chemical and X-ray analysis of wood in the two tropical lianas Bauhinia guianensis and Condylocarpon guianense: variations during ontogeny". In: *Planta* 217.1 (2003), pp. 32–40.

[32] Meriem Fournier et al. "Tree biomechanics and growth strategies in the context of forest functional ecology". In: *Ecology and biomechanics: a mechanical approach to the ecology of animals and plants* (2006), pp. 1–34.

[33] Renaud Bastien, Stéphane Douady, and Bruno Moulia. "A unifying modeling of plant shoot gravitropism with an explicit account of the effects of growth". In: *Frontiers in plant science* 5 (2014), p. 136.

[34] Roland Ennos. *Solid biomechanics.* Princeton University Press, 2011.

[35] Karl J Niklas and Hanns-Christof Spatz. *Plant physics.* University of Chicago Press, 2012.

[36] Peter B Kaufman, Sandra J Cassell, and Paul A Adams. "On nature of intercalary growth and cellular differentiation in internodes of Avena sativa". In: *Botanical Gazette* 126.1 (1965), pp. 1–13.

[37] Sarah M McKim. "Moving on up–controlling internode growth". In: *new phytologist* 226.3 (2020), pp. 672–678.

[38] Nicholas P. Rowe et al. "Diversity of mechanical architectures in climbing plants: an ecological perspective". In: *Ecology and biomechanics: a mechanical approach to the ecology of animals and plants* 35 (2006), p. 59.

[39] Steve Wolff-Vorbeck et al. "Charting the twist-to-bend ratio of plant axes". In: *Journal of the Royal Society Interface* 19.191 (2022), p. 20220131.